This article was downloaded by:
On: *14 January 2011*
Access details: *Access Details: Free Access*
Publisher *Taylor & Francis*
Informa Ltd Registered in England and Wales Registered Number: 1072954 Registered office: Mortimer House, 37-41 Mortimer Street, London W1T 3JH, UK

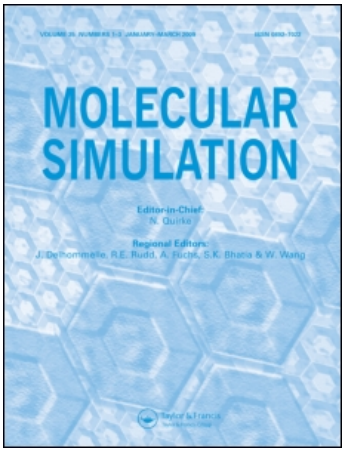

Molecular Simulation
Publication details, including instructions for authors and subscription information:
http://www.informaworld.com/smpp/title~content=t713644482

The Interaction of Fluids with Nanomaterials: Contact Angles at Nanopatterned Interfaces

M. Schneemilch; N. Quirke

Online publication date: 13 May 2010

To cite this Article Schneemilch, M. and Quirke, N.(2003) 'The Interaction of Fluids with Nanomaterials: Contact Angles at Nanopatterned Interfaces', Molecular Simulation, 29: 10, 685 — 695
To link to this Article: DOI: 10.1080/0892702031000103248
URL: http://dx.doi.org/10.1080/0892702031000103248

PLEASE SCROLL DOWN FOR ARTICLE

Full terms and conditions of use: http://www.informaworld.com/terms-and-conditions-of-access.pdf

This article may be used for research, teaching and private study purposes. Any substantial or systematic reproduction, re-distribution, re-selling, loan or sub-licensing, systematic supply or distribution in any form to anyone is expressly forbidden.

The publisher does not give any warranty express or implied or make any representation that the contents will be complete or accurate or up to date. The accuracy of any instructions, formulae and drug doses should be independently verified with primary sources. The publisher shall not be liable for any loss, actions, claims, proceedings, demand or costs or damages whatsoever or howsoever caused arising directly or indirectly in connection with or arising out of the use of this material.

Molecular Simulation, VOL. 29 (10–11), October–November 2003, pp. 685–695

Taylor & Francis
Taylor & Francis Group

The Interaction of Fluids with Nanomaterials: Contact Angles at Nanopatterned Interfaces

M. SCHNEEMILCH and N. QUIRKE*

Department of Chemistry, Imperial College of Science, Technology and Medicine, South Kensington, SW7 2AY, UK

(Received November 2002; In final form December 2002)

We report an extensive set of results for the contact angles of wetting fluids at striped nanopatterned surfaces. We consider the contact angle perpendicular and parallel to the stripe pattern as a function of coverage, wavelength and energy contrast. The contact angle perpendicular to the stripe, where a hemicylindrical region of liquid is in effect pinned at or close to the pattern edge, is determined by the coverage and pattern geometry but is unrelated to the Youngs or Cassie law contact angle. It can be predicted by minimal models of the surface free energy. Above a given surface energy and coverage, the surface coverage unbends to a planar wetting film. The contact angle parallel to the stripe in contact with the vapour liquid boundary varies across the pattern as a function of wavelength (at fixed coverage) tending to a Cassie law value at low wavelength for low contrast patterns. However Cassie's law breaks down for high contrast patterns.

Keywords: Young's equation; Cassie law; Wetting; Contact angle

Downloaded At: 18:37 14 January 2011

INTRODUCTION

Microscale devices based on fluid flows have significant advantages over their macroscale analogs [1–3] arising for example from laminar flows and very large surface to volume ratios. This enables novel microscale sensors, parallelisation, small sample volumes and high speed [4,5]. The key to success is to be able to direct (by, for example, channelling, by external fields or by wetting contrast) and pump fluids on a small scale and this has created a tremendous interest in fluid motion on the microscale or microfluidics [6]. In parallel with developments in microfluidics there is now huge investment in nanomaterials and in their use in nanotechnologies with the total investments worldwide amounting to some $1.6 billion (2001) in new facilities and existing centres of excellence [7]. Clearly, the advantages gained by creating devices at the microscale will in many cases be increased a 1000-fold if they can be constructed at the nanoscale: small volumes and speed should scale quite naturally. However, moving to the nanoscale also introduces new phenomena which have the potential to transform devices and applications; miniaturization to sub-micron dimensions, to nanofluidics, allows the properties of surfaces and their physics and chemistry to dominate the flow (indeed our most recent work has demonstrated the sensitivity of nanopore flow to surface structure [8,9]). One important aspect of the influence of surfaces on fluids is the phenomenon of wetting, the spreading or otherwise of fluids on a surface. It is of interest, for example, to investigate the validity of classical capillarity for the contact angle and surface tension of heterogeneous surfaces, i.e. Cassie's law [10,11].

In previous work [12], we have investigated the validity of Cassie's law for the surface tension of heterogeneous surfaces. A variety of statistical mechanical sum rules are employed to measure the interfacial free energies and a set of interfacial order parameters associated with patterned inhomogeneous fluids. We directly observed two classes of interfacial phase transitions: (i) an unbending transition at the solid–vapour interface, which must precede complete wetting in systems where low-energy regions are not completely wet, (ii) a surface crystallization-layering transition associated with a hemicylindrical region of enhanced liquid structure

*Corresponding author.

ISSN 0892-7022 print/ISSN 1029-0435 online © 2003 Taylor & Francis Ltd
DOI: 10.1080/0892702031000103248

at the substrate-liquid boundary. For a vapour phase in contact with a striped surface we observed hemicylindrical drops pinned to the stripe boundaries, with a mechanical contact angle unrelated to that defined by Young's equation. The magnitude and variation of the mechanical contact angle with system parameters can be understood from minimal models of adsorption on patterned surfaces.

In what follows we extend our study of the static wetting properties of a fluid in contact with a solid surface, developing our minimal models by incorporating simulation data for pinned drop properties as well as reporting new simulation data for three phase wetting of surfaces with multiple stripes. We concentrate on the value of the contact angle as measured by fits to density profiles of wetting fluids, perpendicular and parallel to the stripe pattern.

The free energy of a saturated adsorbed film is often analysed in terms of Young's contact angle θ, defined from statistical mechanics as

$$\gamma_{\mathrm{lv}} \cos\theta = \gamma_{\mathrm{sv}} - \gamma_{\mathrm{sl}}. \tag{1}$$

In thermodynamic equilibrium $-1 \leq \cos\theta \leq 1$, with $\cos\theta = 1$ corresponding to a macroscopically thick adsorbed film of liquid (since then $\gamma_{\mathrm{sv}} = \gamma_{\mathrm{sl}} + \gamma_{\mathrm{lv}}$) termed complete wetting. Otherwise the interface is said to exhibit partial wetting by liquid. For partial wetting on a chemically patterned substrate it is important to note that Young's mechanical interpretation of the contact angle, in terms of the visual angle made by the surface of an adsorbed drop of excess liquid, is not appropriate if the excess liquid is pinned to the pattern boundary [10,11]. In the discussion below θ will always refer to the statistical mechanical definition, while any "visually" observed contact angle will be denoted θ_m.

Downloaded At: 18:37 14 January 2011

METHOD

Simulation

The fluid–fluid interaction is taken to be a truncated and shifted Lennard–Jones model:

$$u(r) = 4\varepsilon\left[\left(\frac{\sigma}{r}\right)^{12} - \left(\frac{\sigma}{r}\right)^{6} - \left(\frac{\sigma}{r_c}\right)^{12} + \left(\frac{\sigma}{r_c}\right)^{6}\right] \qquad r < r_c, \tag{2}$$

with $\varepsilon/k_{\mathrm{B}} = 94.95\,\mathrm{K}$ (k_{B} denotes Boltzmann's constant), $\sigma = 0.3549\,\mathrm{nm}$ and $r_c = 1.05\,\mathrm{nm}$, which could be regarded as a model of molecular nitrogen. At temperature $T = 77\,\mathrm{K}$, or $T^* \equiv k_{\mathrm{B}}T/\varepsilon = 0.81$, the liquid–vapour surface tension of this fluid, in standard reduced units, is $\gamma^*_{\mathrm{lv}} \equiv \gamma_{\mathrm{lv}}\sigma^2/\varepsilon = 0.53 \pm 0.04$. All our data reported below were collected at this single temperature, which lies roughly one quarter of the way from the triple point to the liquid–vapour critical point T_c.

Vertically above any portion of a chemically patterned, but otherwise planar, surface, we take the solid–fluid potential to be [12]

$$u_{\mathrm{sf}}(z) = 2\pi\varepsilon_{\mathrm{sf}}\left[\frac{2}{5}\left(\frac{\sigma_{\mathrm{sf}}}{z}\right)^{10} - \left(\frac{\sigma_{\mathrm{sf}}}{z}\right)^{4} - \frac{\sigma_{\mathrm{sf}}^4}{3\Delta(z+0.61\Delta)^3}\right], \tag{3}$$

where $\sigma_{\mathrm{sf}} = 0.347\,\mathrm{nm}$, $\Delta = 0.335\,\mathrm{nm}$ and $\varepsilon_{\mathrm{sf}}$ is the solid–fluid intermolecular well depth relevant to that portion of the surface. The choice of $\varepsilon_{\mathrm{sf}}$ determines whether the interaction with the surface is strong or weak compared to the fluid–fluid interaction ε and the thermal energy $k_{\mathrm{B}}T$. In subsequent discussion we employ a dimensionless ratio ε_r, obtained by dividing the minimum of the solid–fluid potential $-u_{sf}(z_{\min})$ by ε. Dimensionless lengths, denoted by a * superscript, are obtained by dividing by σ. Chemically patterned surfaces are created by placing one or more high-energy stripes ε_r on a background surface with $\varepsilon_b < \varepsilon_r$, then using periodic boundary conditions to mimic an infinite array of stripes. The interface between adjoining regions is treated as sharp, i.e. we choose a simple discontinuous change from ε_b to ε_r Although this latter choice is not fully consistent with the derivation of Eq. (3), it does have the benefit of generating particularly clear statistical mechanical sum rules. The notation below assumes that the chemical stripes are oriented parallel to the y-axis and the parameter λ denotes the wavelength of the pattern.

Denoting the width of the high energy stripe by w, we define the fraction of the wall area covered by high energy surface (the coverage c) by $w = c\lambda$. The classical theory of adsorption on chemically patterned surfaces is due to Cassie [10,11]. Cassie's law assumes that the interfacial free energy of a planar heterogeneous interface is a simple sum of contributions from individual regions, which themselves behave as if they were of infinite extent (denoted below with a superscript ∞) [13]. For our striped patterns this implies

$$\gamma_{\mathrm{sf}} = c\gamma^{\infty}_{\mathrm{rf}} + (1-c)\gamma^{\infty}_{\mathrm{bf}}, \tag{4}$$

with $f \in \{l, v\}$ and, as before, r and b denote the high energy stripe surface and the low energy background surface, respectively. When combined with Eq. (1) this would lead us to conclude

$$\cos\theta = c\cos\theta^{\infty}_r + (1-c)\cos\theta^{\infty}_b. \tag{5}$$

Two different starting configurations were employed to simulate the properties of fluids in equilibrium with these surfaces, both containing a total of 2048 fluid particles. In the first configuration

(C1), Fig. 1a, a slab of liquid was placed in one half of a simulation cell bounded on opposite sides by identical walls of dimension $L_x = L_y = 14\sigma$, separated by a distance $L_z = 28\sigma$, and periodic in the remaining orthogonal directions. The liquid then equilibrates forming a liquid–vapour interface in the centre of the cell, with a saturated liquid phase adsorbed at one end and a vapour phase at the other. The presence of the liquid–vapour interface ensures liquid vapour coexistence (at $T < T_c$) as we vary the surface properties of the walls, which are sufficiently far apart to regard as independent. Thus, broken symmetry is imposed by the starting configuration C1. Symmetry is restored following a transition to complete wetting at the wall–vapour interface or complete drying at the wall–liquid interface [14–16]. Although the total number of particles is fixed, a canonical ensemble, each of the three interfacial regions and two bulk regions approximate a subsystem of a Grand ensemble, due to the interchange of particles between them. Data reported below were typically averaged over 10 subruns of 15×10^6 trial moves each and error bars shown are the standard deviations of the 10 subruns. Equilibration times ranged from 150 to 900×10^6 trial moves. In certain situations such as near a transition to complete wetting the equilibration was enhanced by increasing the maximum attempted displacement of the Monte Carlo moves, over a single subrun [17]. This reduces the time taken for particles to migrate across the cell from the liquid phase to the wall–vapour interface that would be prohibitively long in molecular dynamics simulations [18–20]. Figure 1b shows density contours at a wall–vapour interface above a relatively low energy stripe, well away from unbending and surface crystallisation-layering. For $\varepsilon_r = 3.5$ one clearly observes the formation of hemicylindrical drops on top of the high energy stripe. This structure remains at higher stripe energies, unless overtaken by an unbending transition, following unbending the liquid–vapour interface of the adsorbed film adopts a planar configuration, no longer modulated by the underlying substrate pattern. It is important to note that

Downloaded At: 18:37 14 January 2011

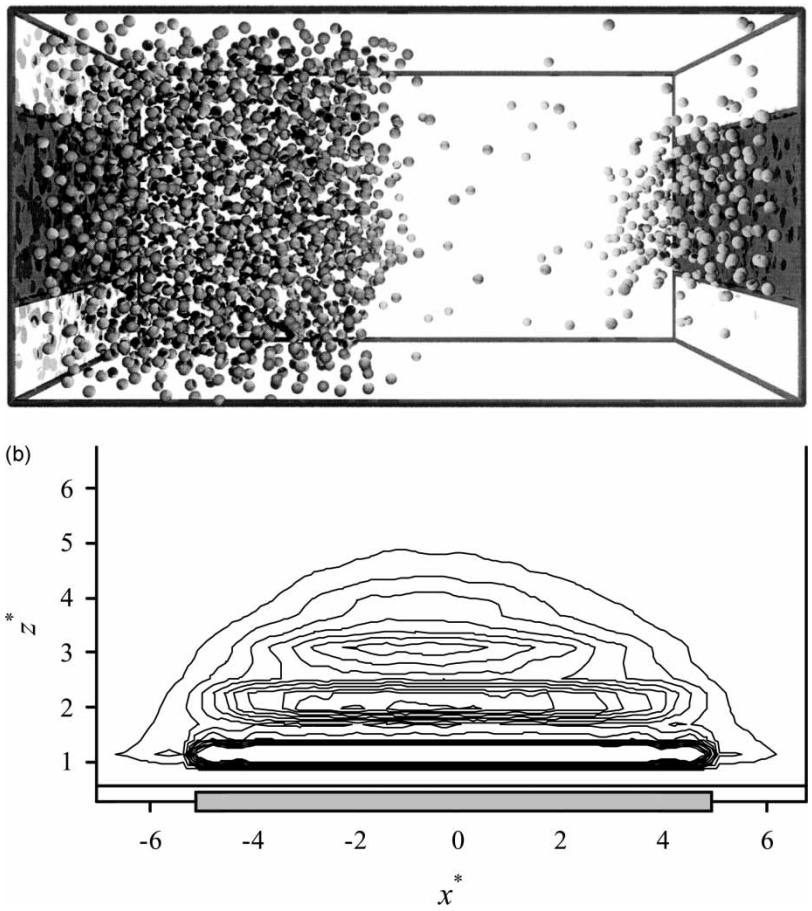

FIGURE 1 (a) Configuration c1 of the simulations. A slab of liquid was placed in one half of a simulation cell bounded on opposite sides by identical walls of dimension $L_x = L_y = 14\sigma$, separated by a distance $L_z = 28\sigma$, and periodic in the remaining orthogonal directions. The liquid equilibrates forming a liquid–vapour interface in the centre of the cell, with a saturated liquid phase adsorbed at one end and a vapour phase at the other. (b) Typical density contours for the vapour adsorbed onto the high energy stripe, $c = 0.7$, $\lambda = 14\sigma$, $\varepsilon_r = 3.5$. The position of the stripe is shown by the thick grey line on the x axis.

the apparent contact angle θ_m made by the drop has no relation to Young's equation (1). In fact, this mechanical contact angle does not change significantly with ε_r but instead has a value determined by the pattern geometry as discussed below. It is also interesting to note that hemicylindrical density contours are equally apparent in wall–liquid profiles [12].

In the second configuration [21], (C2), Fig. 2, one side of the system was increased to $L_x = 42\sigma$ with L_y remaining at 14σ, while the separation between the walls was reduced to $L_z = 14\sigma$. The fluid particles were initially placed in a slab centred in the middle of the cell, such that it was in contact with both walls.

In both C1 and C2 a contact angle can be measured directly by fitting the liquid–vapour interface profile, obtained from lines of constant density, to an arc of a circle [21]. In both cases the contact angle is measured in a plane perpendicular to the wall; in C1 it is the plane perpendicular to the long axis of the stripe on the vapour side of the system, $\theta_m = \theta_m^{\perp}$, while in C2 the plane is parallel to the stripe, $\theta_m = \theta_m{}''$.

Minimal Models

Following Rascón and Parry [22], we have developed [12] a minimal model of the wetting of a patterned surface when the adsorbed liquid is pinned to the pattern in the form of hemispherical drops as observed in the simulations. Defining $h(x)$ to be the height of the liquid–vapour interface above the striped substrate, the equilibrium shape of an adsorbed film of liquid is obtained by minimising the free energy functional

$$F[h] = \frac{L_x L_y}{\lambda} \int_{-\lambda/2}^{\lambda/2} \mathrm{d}x \frac{1}{2} \gamma \left(\frac{\mathrm{d}h}{\mathrm{d}x} \right)^2 + F_r[h_d] + F_b[h_b]. \quad (6)$$

The first term in this free energy, (denoted $L_x L_y\, I$ below), is the contribution from the bending of the (drop) liquid–vapour interface, due to the liquid film being strongly influenced by the underlying chemical pattern. The final two terms are the free energies of planar films, adsorbed on a high energy substrate (ε_r) and a low energy substrate (ε_b), respectively. Our minimal model restricts the minimisation of Eq. (6) to the idealised geometry of Fig. 3, in which liquid films of height h_d and h_b are adsorbed in the form of hemicylindrical drops on top of a planar background film. The drops make a contact angle $\theta_m \equiv \theta_m^{\perp}$ with the background and have a horizontal extent Λ that need not be identical to the width w of the high energy stripe, Fig. 3. In Ref. [12] Eq. (6) is solved for stripes for which

$$h_d - h_b = R(1 - \cos\theta_m) = \frac{\Lambda}{2\sin\theta_m}(1 - \cos\theta_m)$$
$$\equiv \Lambda J(\theta_m). \quad (7)$$

The solid–vapour surface tensions are obtained from a Taylor series expansion about the homogenous solutions denoted by superscript ∞, and

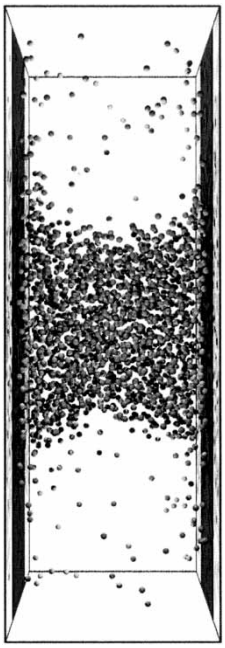

FIGURE 2 Configuration C2 of the simulations. Starting from the cell of C1, one side of the system was increased to $L_x = 42\sigma$ with L_y remaining at 14σ, while the separation between the walls was reduced to $L_z = 14\sigma$. The fluid particles were initially placed in a slab centred in the middle of the cell, such that it was in contact with both walls.

Downloaded At: 18:37 14 January 2011

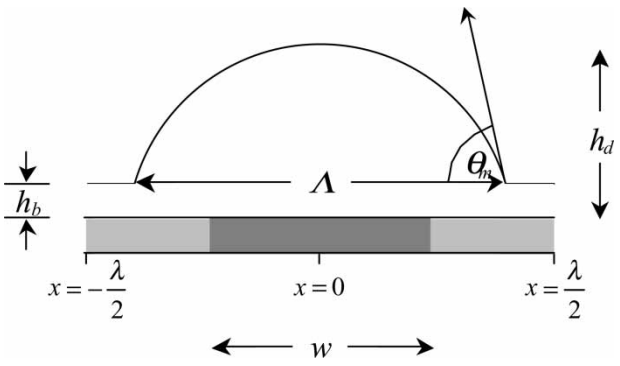

FIGURE 3 Idealised hemicylindrical drops adsorbed on a striped surface. The drops (of width Λ) form over the high energy stripes (width w) and reach a maximum height h_d. Over the background low-energy regions of the surface the fluid adsorbs as a thin film of height h_b. The hemicylindrical drops make a contact angle θ_m with the background film.

the total free energy of the adsorbed film, per unit planar surface area, becomes

$$f[h] = I + c_d[\gamma_{\mathrm{rv}}^{\infty} + \frac{1}{2}\gamma_{\mathrm{rv}}''(h_d - h_d^{\infty})^2] + (1 - c_d) \times [\gamma_{\mathrm{bv}}^{\infty} + \frac{1}{2}\gamma_{\mathrm{bv}}''(h_b - h_b^{\infty})^2, \quad (8)$$

where we have introduced $c_d \equiv \Lambda/\lambda$. Note that c_d is the coverage of the surface by hemicylindrical drops, to in general be distinguished from c the coverage of the surface by high energy stripes.

We now look for simultaneous solutions to $\partial f/\partial h_i = 0$; $i \in \{r, b\}$, at fixed c_d giving

$$g(\theta_m) + (\beta_r/\alpha)(h_d - h_d^{\infty}) = 0, \quad (9)$$

$$-g(\theta_m) + (\beta_b/\alpha)(h_b - h_b^{\infty}) = 0, \quad (10)$$

with $\alpha \equiv \gamma/\lambda$, $\beta_r \equiv c_d\gamma_{\mathrm{rv}}''$, $\beta_b \equiv (1 - c_d)\gamma_{\mathrm{bv}}''$ and

$$g(\theta_m) \equiv \frac{\tan\theta_m}{1 - \cos\theta_m} - \frac{\cos\theta_m}{2(1 - \cos\theta_m)} \ln\left(\frac{1 + \sin\theta_m}{1 - \sin\theta_m}\right).$$

Adding these equations gives

$$\beta_r(h_d - h_d^{\infty}) + \beta_b(h_b - h_b^{\infty}) = 0, \quad (11)$$

so that we can express the equilibrium film heights as

$$h_d - h_d^{\infty} = \frac{-\beta_b}{\beta_r + \beta_b}(-\Lambda J(\theta_m) + h_d^{\infty} - h_b^{\infty}), \quad (12)$$

$$h_b - h_b^{\infty} = \frac{\beta_r}{\beta_r + \beta_b}(-\Lambda J(\theta_m) + h_d^{\infty} - h_b^{\infty}), \quad (13)$$

and

$$g(\theta_m) = \frac{\beta_r\beta_b}{\alpha(\beta_r + \beta_b)}(-\Lambda J(\theta_m) + h_d^{\infty} - h_b^{\infty}). \quad (14)$$

The method of solution [12], therefore, requires one to choose suitable values for α, β_r, β_b, Λ (or c_d), h_d^{∞} and h_b^{∞}, and then substitute into Eq. (14) to obtain θ_m. This, in turn, gives the height of the drop and the thickness of the background film, by substituting into Eqs. (12) and (13).

RESULTS

The Contact Angle $\theta_m = \theta_m^{\perp}$

In configuration C1 for $\varepsilon_r = 3.5$ one clearly observes the formation of hemicylindrical drops on top of the high energy stripe (Fig. 1b). This structure remains at higher stripe energies, unless overtaken by an unbending transition [12]. It is important to note that the apparent contact angle $\theta_m^{\perp}$ made by the drop has no relation to Young's equation. At the high coverage $c = 0.9$ the lateral stress involved in maintaining a hemicylindrical drop profile is released by the system undergoing an unbending transition seen, in particular, in Fig. 4. Following unbending the liquid–vapor interface of the adsorbed film adopts a planar configuration, no longer modulated by the underlying substrate pattern. Note that hemicylindrical density contours are equally apparent in wall–liquid profiles. In configuration C1 on the vapour side the contact angle is therefore, a strong function of the coverage c of the surface. The contact angle does not change significantly with ε_r (unless unbending intervenes) but instead has a value determined by the pattern geometry $\theta_m^{\perp} \approx 74°$ for $c = 0.5$ and 60° for $c = 0.7$. In Ref. [10,11] this contact angle variation as a function of coverage was predicted using the minimal model described above with the approximation of complete pinning, i.e. $\Lambda = w$, $c_d = c$. Due to the simplicity of the model, unbending occurs strictly at $c = 1$ without undergoing a true interfacial phase transition, however, the tendency as a function of coverage is otherwise physically correct. Nevertheless the data in Fig. 5a for Λ, the drop width shows that $\Lambda > w$ and thus the assumption of complete pinning is rather drastic. In addition in order to fit the simulation data it was assumed that $\gamma^* = 2$. This last value of the surface tension of the pinned drop is unrealistic given that the liquid vapour surface tension measured using the pressure tensor across the planar liquid vapour interface on the liquid side, $\gamma_{\mathrm{lv}}^* = 0.53$, is almost four times smaller. In order to improve the fit we relax the complete pinning approximation and use the mean values of the data of Fig. 5a for Λ (c) as input to the model (for $c_d = 0.7$ only those $\Lambda \leq \lambda$ were used to obtain the mean), ignoring corrections to the free energies due to overlap. In Fig. 5b we plot the predicted pinned contact angles. Despite the approximations in the model it predicts the correct trends, where now $\gamma^* = \gamma_{\mathrm{lv}}^* = 0.53$.

Downloaded At: 18:37 14 January 2011

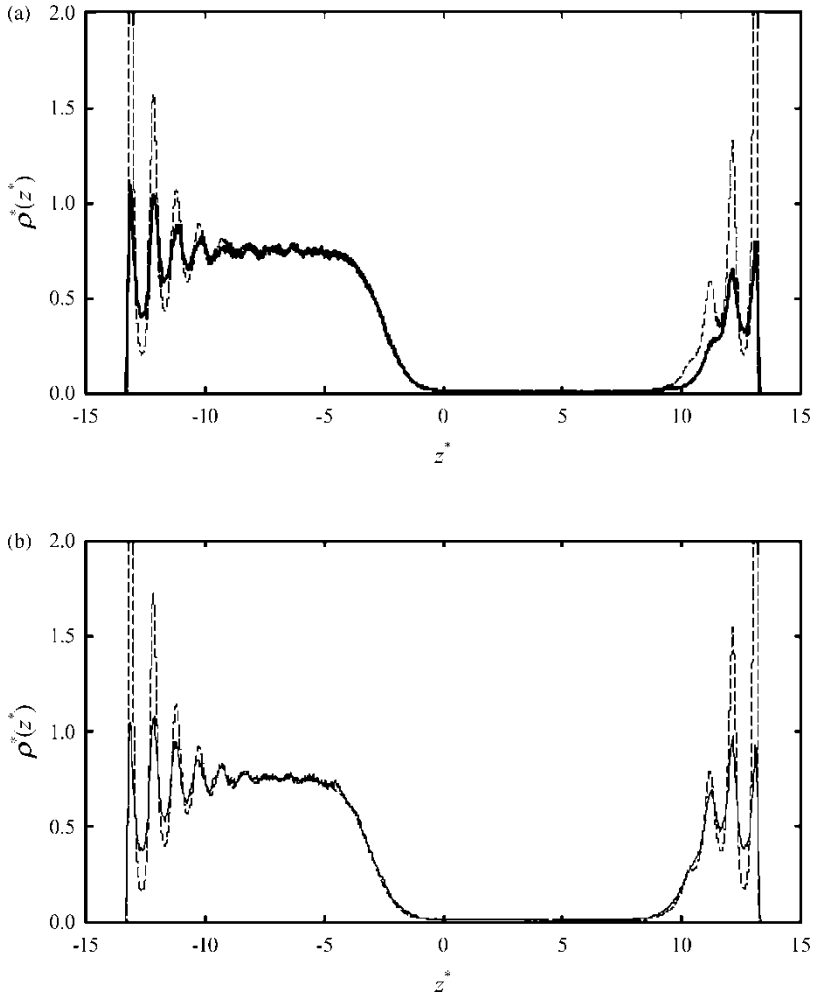

Downloaded At: 18:37 14 January 2011

FIGURE 4 (a) Density profiles for configuration C1: $c = 0.9$, $\lambda = 14\sigma$, $\varepsilon_r = 4.1$, thick line above the background, dashed line above the stripe. Clearly there is a bent profile on the vapour side where the third peak in the profile is missing from the background film. (b) Density profiles for configuration C1: $c = 0.9$, $\lambda = 14\sigma$, $\varepsilon_r = 4.5$, thick line above the background, dashed line above the stripe. The two profiles on the vapour side are now similar and the adsorbed film has unbent.

The Contact Angle $\theta_m = \theta_m''$

In our previous publication we reported values of the contact angle for the homogeneous surfaces. For the background, the contact angle was $112 \pm 6°$, while the surface at $\varepsilon_r = 2.9$ had just undergone the wetting transition, $\theta = 0°$. These values were obtained from Young's equation, using values of the surface–fluid interfacial tensions calculated during Monte Carlo simulations by the mechanical route in configuration 1. Direct measurement of the contact angle in configuration C2 was in good agreement with these data.

In the configuration C2 the liquid vapour contact line runs across the stripes so that the contact angle can be measured in the direction parallel to the stripes. Figure 6 shows the contact angle profiles across the surface for increasing number of stripes (decreasing wavelength) at constant coverage, $c = 0.5$. The single stripe system is completely wet [12] in the centre of the stripe and reaches the homogeneous background value in the centre of the background. As we increase the number of stripes the variation across the surface is reduced until with four stripes the contact angle is effectively constant (63 ± 3) and equal to the Cassie law value (69 ± 8). In these figures the Cassie's law value is shown as a solid horizontal line. Also shown (dashed line) is the value calculated from Young's equation using surface tension values obtained from the mechanical route in configuration 1. When the stripe energy is 2.9 the Young's equation value agrees with Cassie's Law. If we increase ε_r to $\varepsilon_r = 4.1$ then for a single stripe (Fig. 7a) the entire stripe region is completely wet, $\theta_m'' = 0$. This is confirmed by the density contours in Fig. 7c along the middle of the stripe, in contrast the background again has a constant angle of ~ 100 with the non-contact surface completely dry. In moving across this dry surface perpendicular to the stripes we encounter the completely wet stripe with a pinned contact angle $\theta_m^{\perp}$ as discussed in the previous section. Increasing the number of stripes to two (Fig. 8) again increases

Downloaded At: 18:37 14 January 2011

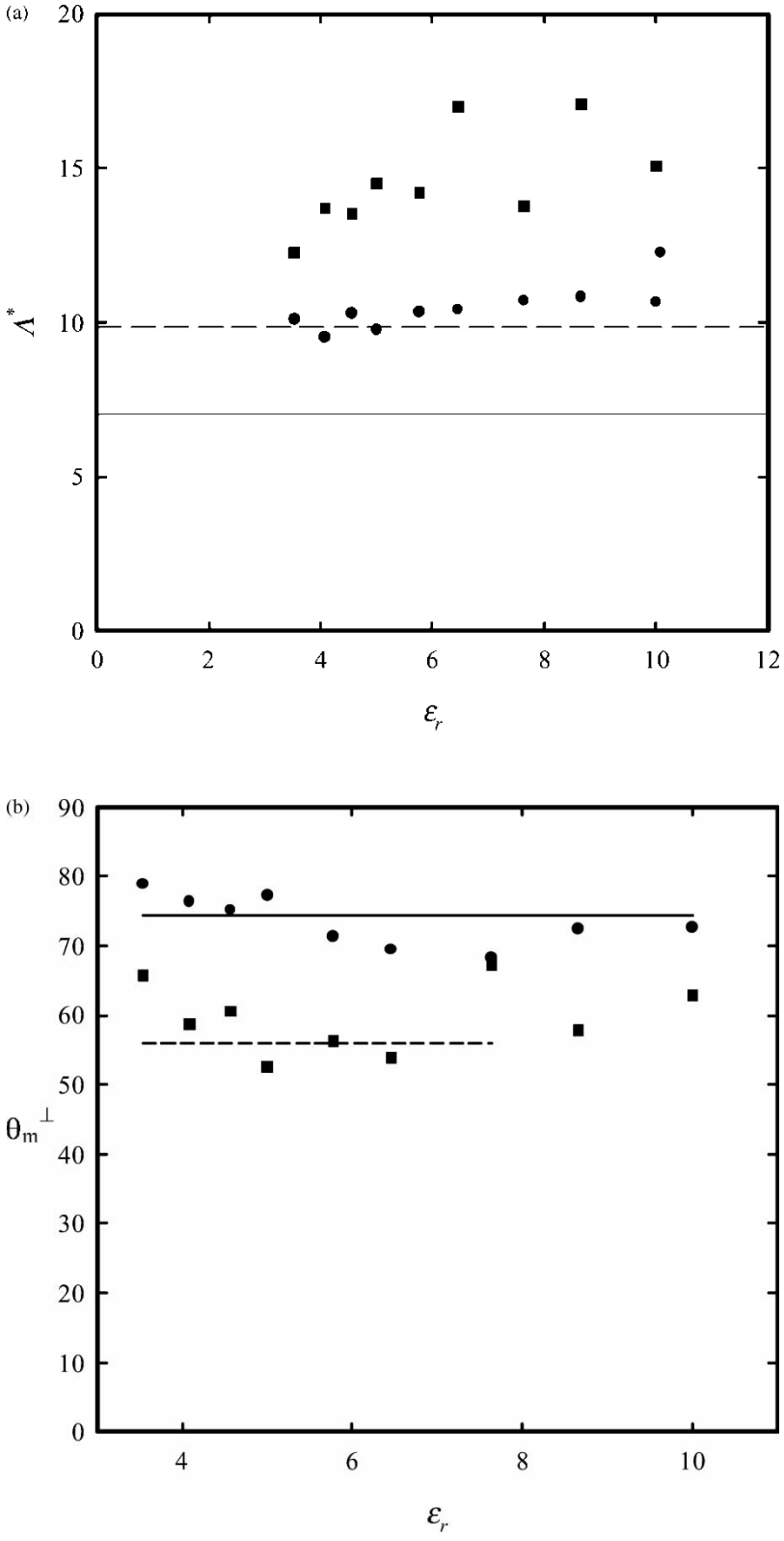

FIGURE 5 Parameters for the minimal model from simulation (symbols, obtained from fitting circular profiles to density profiles) and theory (lines, setting $\lambda = 4\sigma$, $\gamma^* = 0.53$, $\gamma_{rv}'' = \gamma_{bv}'' = 1$, $h_d^\infty = 4.4\sigma$ and $h_b^\infty = 0.1\sigma$). ●: $w^* = 7$ (solid line), ■: $w^* = 9.8$ (dash line). (a) Drop width, Λ; (b) Pinned contact angles.

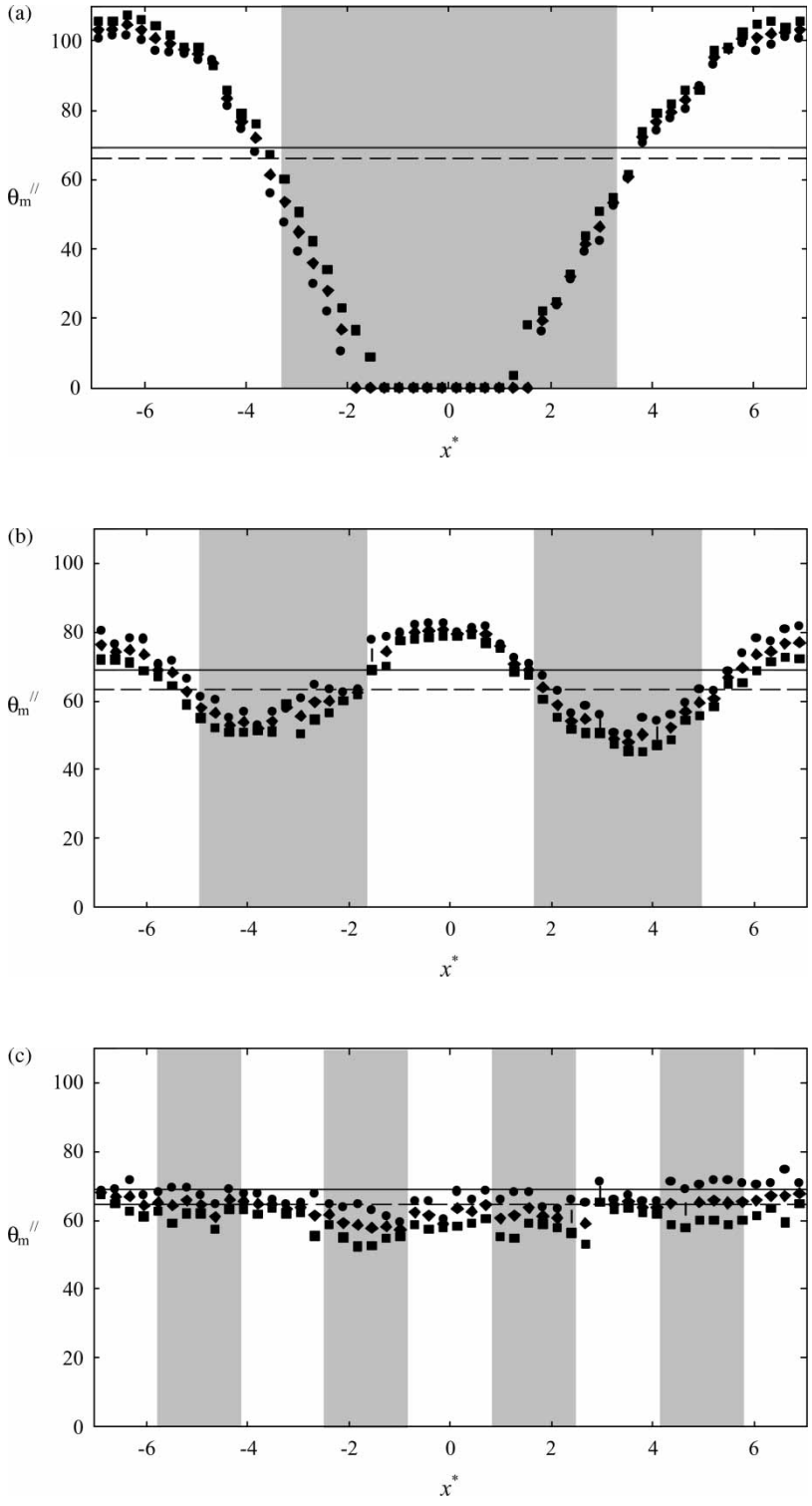

FIGURE 6 (a) The contact angle measured in configuration C2 along the stripe $\theta_m{}''$ for $\varepsilon_r = 2.9$, $c = 0.5$, single stripe. Filled squares lower surface, filled spheres upper surface, filled diamonds average, solid line Cassie's law value, dashed line Young's equation. (b) The contact angle measured in configuration C2 along the stripe $\theta_m{}''$ for $\varepsilon_r = 2.9$, $c = 0.5$, double stripe. Filled squares lower surface, filled spheres upper surface, filled diamonds average, solid line Cassie's law value, dashed line Young's equation. (c) The contact angle measured in configuration C2 along the stripe $\theta_m{}''$ for $\varepsilon_r = 2.9$, $c = 0.5$, four stripes. Filled squares lower surface, filled spheres upper surface, filled diamonds average, solid line Cassie's law value, dashed line Young's equation.

Downloaded At: 18:37 14 January 2011

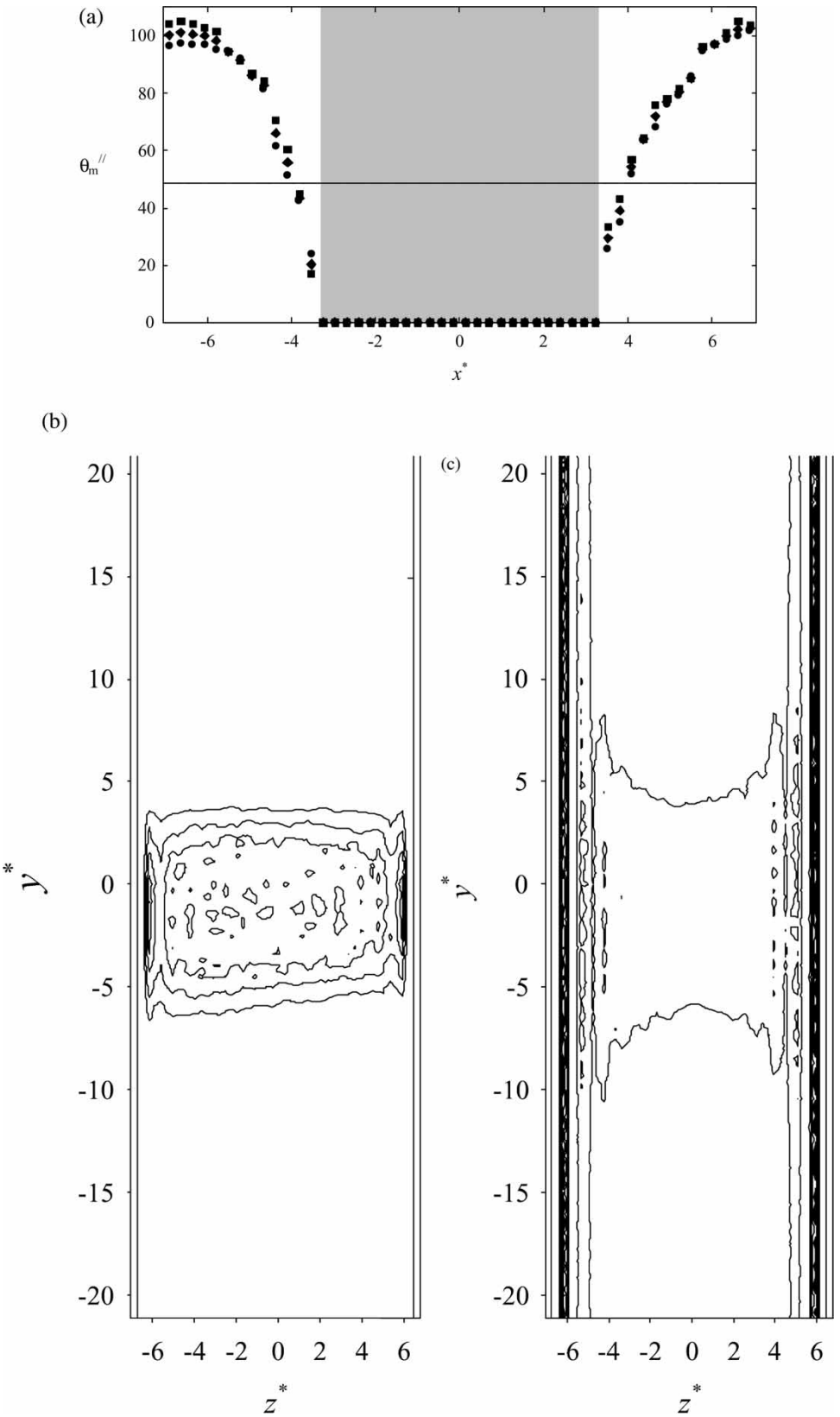

FIGURE 7 (a) The contact angle measured in configuration C2 along the stripe $\theta_m{}''$ for $\varepsilon_r = 4.1$, $c = 0.5$, single stripe. Filled squares lower surface, filled spheres upper surface, solid line Cassie's law value, dashed line Young's equation. (b) Density profile along background corresponding to $x^* = -6.9$ in Fig. 7a (large contact angle). (c) Density profile along background corresponding to $x^* = 0$ in Fig. 7a (zero contact angle).

Downloaded At: 18:37 14 January 2011

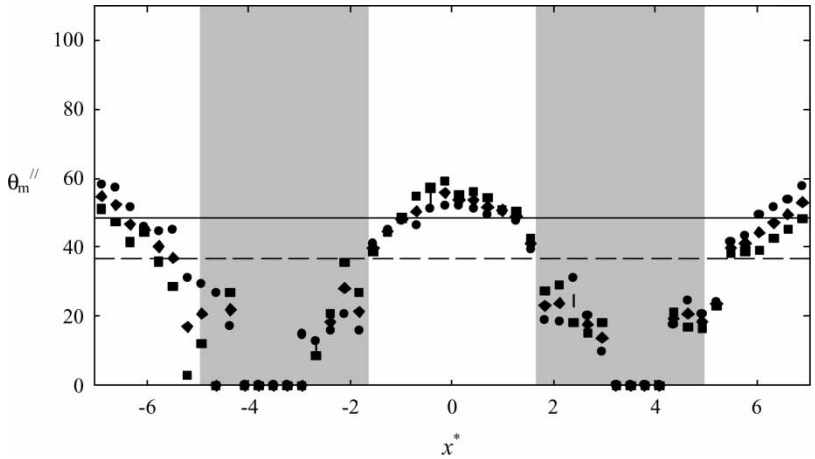

FIGURE 8 The contact angle measured in configuration C2 along the stripe θ_m'' for $\varepsilon_r = 4.1$, $c = 0.5$, double stripe. Filled squares lower surface, filled spheres upper surface, filled diamonds average, solid line Cassie's law value, dashed line Young's equation.

the contact angle on the stripe and reduces the background contact angle. Now the Young's equation value (37°) is lower than the Cassie's law value (48.5 ± 12°). Note that to calculate the Cassie law value we have used the metastable contact angles ($\cos\theta > 1$) found for the homogeneous surfaces, if we take $\cos\theta = 1$ then the Cassie law angle is 69 ± 8 as before. When the stripe energy is increased to 4.1 in the four stripe system both stripe and background are completely wet. For this system the apparent contact angle (0°) is well below the Cassie value, however calculated, but agrees with the prediction of complete wetting obtained from Young's equation. This is consistent with the observation by Drelich *et al.* [23] that Cassie's law fails for high energy contrast surfaces.

CONCLUSIONS

We report an extensive set of computer simulation data for the adsorption of saturated vapour at chemically striped planar walls, over a wide range of energy contrast between the pattern regions.

At wall–vapour interfaces, i.e. perpendicular to the stripe, we observe lateral stress arising from the hemicylindrical drop pattern, which is released at the unbending transition proposed by Parry and coworkers [22,24–27] and similar to the morphological wetting transition of Lenz and Lipowsky [28], except that the latter impose a constraint of constant liquid volume. Unbending is favoured by increasing the percentage of high energy regions and by decreasing the pattern wavelength.

Parallel to the stripe at the liquid/vapour interface the contact angle varies across the surface as a function of the pattern wavelength in an approximately sinusoidal manner. As the wavelength decreases at fixed coverage the contact angle tends to that predicted by Cassie's law for $\varepsilon_r = 2.9$ but for higher contrasts the situation becomes more complex with several different contact angles evident. When the stripe energy is raised to $\varepsilon_r = 4.1$ deviations from Cassie's law become increasingly evident as the wavelength is decreased. The contact angle goes to zero for the four stripe system as predicted by Young's equation.

Finally, we note the simplified free energy model introduced by us in Ref. [12] predicts the perpendicular contact angle as a function of both energy contrast and coverage with physically reasonable parameters if the drop width from the simulations is used as an input parameter. Note that this model is too simplified to display unbending as a true phase transition. Both computer simulation and theory, therefore, predict that laterally inhomogeneous adsorption profiles should be observed in future experiments on the wetting of nanopatterned substrates.

Acknowledgements

We thank EPSRC for support through grants GR/N64809 and GR/M94427 and Dr J Henderson for useful discussions.

References

[1] Terry, A., Oakey, J. and Marr, D.W.M. (2002) "Microfluidic control using colloidal devices", *Science* **296**, 1841.
[2] Effenhauser, C.S., Manz, A. and Widmer, H.M. (1993) "Glass chips for high-speed capillary electrophoresis separations with submicrometer plate heights", *Anal. Chem.* **65**, 2637.
[3] Wilding, P., Shoffner, M.A. and Kricka, L.J. (1994) "PCR in a silicon microstructure", *Clin. Chem.* **40**, 1815.
[4] Whitesides, G.M. and Stroock, A.D. (2001) "Flexible methods in microfluidics", *Phys. Today* **54**, 42.
[5] Kopp, M.U., de Mello, A.J. and Manz, A. (1998) "Chemical amplification: continuous-flow PCR on a chip", *Science* **280**, 1046.

Downloaded At: 18:37 14 January 2011

[6] van den Berg, A., Olthuis, W. and Bergveld, P. (2000) *Micro Total Analysis* (Kluwer Academic, Dordretch, Netherlands).
[7] Roco, M.C. (2002) "The vision and action plan of the National Nanotechnology Initiative", *Comput. Nanosci. Nanotechnol.*, (www.cr.org) ISBN 0-9708275-6-3.
[8] Sokhan, V.P., Nicholson, D. and Quirke, N. (2001) "Fluid flow in nanopores: an examination of hydrodynamic boundary conditions", *J. Chem. Phys.* **115**, 3878.
[9] Sokhan, V.P., Nicholson, D. and Quirke, N. (2002) "Fluid flow in nanopores: accurate boundary conditions for carbon nanotubes", *J. Chem. Phys.* **117**.
[10] Cassie, A.B.D. (1948), *Faraday Discuss. Soc.* **3**, 11.
[11] Swain, P.S. and Lipowsky, R. (1998), *Langmuir* **14**, 6772.
[12] Schneemilch, M., Henderson, J. and Quirke, N. (2002) "Wetting of nanopatterned surfaces: the striped surface", *J. Chem. Phys.* **118**, 816.
[13] Henderson, J.R. (2000) "Statistical mechanics of Cassie's law", *Mol. Phys.* **98**, 677.
[14] Sikkenk, J.H., Indekeu, J.O., van Leeuwen, J.M.J. and Vossnack, E.O. (1987) "Molecular-dynamics simulations of wetting and drying at solid–fluid interfaces", *Phys. Rev. Lett.* **59**, 98.
[15] Sikkenk, J.H., Indekeu, J.O., van Leeuwen, J.M.J., Vossnack, E.O. and Bakker, A.F. (1988) "Simulation of wetting and drying at solid–fluid interfaces on the Delft molecular dynamics processor", *J. Stat. Phys.* **52**, 23.
[16] Nijmeijer, M.J.P., Bruin, C., Bakker, A.F. and van Leeuwen, J.M.J. (1990), *Phys. Rev., A* **42**, 6052.
[17] Finn, J.E. and Monson, P.A. (1989) "Prewetting at a fluid–solid interface via Monte Carlo simulation", *Phys. Rev. A* **39**, 6402.
[18] van Swol, F. and Henderson, J.R. (1986) "Wetting at a fluid–wall interface: computer simulation and exact statistical sum rules", *J. Chem. Soc. Faraday Trans. II* **82**, 1685.
[19] van Swol, F. and Henderson, J.R. (1991) "Wetting and drying transitions at a fluid–wall interface. Density-functional theory versus computer simulation. II", *Phys. Rev. A* **43**, 2932.
[20] Adams, P. and Henderson, J.R. (1991) "Molecular dynamics simulations of wetting and drying in LJ models of solid fluid interfaces in the presence of liquid–vapour coexistance", *Mol. Phys.* **73**, 1383.
[21] Nijmeijer, M.J.P., Bruin, C., Bakker, A.F. and van Leeuwen, J.M.J. (1989) "A visual measurement of contact angles in a molecular-dynamics simulation", *Physica A* **160**, 166.
[22] Rascón, C. and Parry, A.O. (2001) "Surface phase diagrams for wetting on heterogeneous surfaces", *J. Chem. Phys.* **115**, 5258.
[23] Drelich, J., Wilbur, J.L., Miller, J.D. and Whitesides, G.M. (1996) "Contact angles for liquid drops at a model heterogeneous surface consisting of alternating and parallel hydrophilic/hydrophobic strips", *Langmuir* **12**, 1913.
[24] Swain, P.S. and Parry, A.O. (1998) "Corrugation-induced first-order wetting: an effective Hamiltonian study", *Eur. Phys. J. B* **4**, 459.
[25] Bauer, C., Dietrich, S. and Parry, A.O. (1999) "Morphological phase transitions of thin films on chemically structured substrates", *Eur. Phys. Lett.* **47**, 474.
[26] Parry, A.O., Wood, A.J. and Rascón, C. (2000) "Two-dimensional filling in ordered and disordered systems", *J. Phys. Condens. Matter* **12**, 7671.
[27] Parry, A.O., Wood, A.J. and Rascón, C. (2001) "Wedge filling, cone filling and the strong fluctuation regime", *J. Phys. Condens. Matter* **13**, 4591.
[28] Lenz, P. and Lipowsky, R. (1998) "Morphological transitions of wetting layers on structured surfaces", *Phys. Rev. Lett.* **80**, 1920.

Downloaded At: 18:37 14 January 2011